IEEE Access
Multidisciplinary ⋮ Rapid Review ⋮ Open Access Journal

Received 7 November 2023, accepted 19 January 2024, date of publication 24 January 2024, date of current version 1 February 2024.

Digital Object Identifier 10.1109/ACCESS.2024.3358109

RESEARCH ARTICLE

Spatially Averaged Epithelial/Absorbed Power Density for Nonplanar Skin Models Exposed to Antenna at 10–90 GHz

KUN LI[1], (Member, IEEE), SACHIKO KODERA[2], (Member, IEEE), DRAGAN POLJAK[3], (Senior Member, IEEE), YINLIANG DIAO[4], (Member, IEEE), KENSUKE SASAKI[5], (Member, IEEE), SHUAI ZHANG[6], (Senior Member, IEEE), MING YAO[6], (Graduate Student Member, IEEE), ANTE KAPETANOVIC[3], (Member, IEEE), CONGSHENG LI[7], (Member, IEEE), TONGNING WU[7], (Senior Member, IEEE), THORSTEN LIEBIG[8], WINFRIED SIMON[8], AND AKIMASA HIRATA[2], (Fellow, IEEE)

[1]Advanced Wireless and Communication Research Center, The University of Electro-Communications, Tokyo 182-8585, Japan
[2]Department of Electrical and Mechanical Engineering, Nagoya Institute of Technology, Nagoya 466-8555, Japan
[3]Faculty of Electrical Engineering, Mechanical Engineering and Naval Architecture, University of Split, 21000 Split, Croatia
[4]College of Electronic Engineering, South China Agricultural University, Guangzhou 510642, China
[5]National Institute of Information and Communications Technology, Tokyo 184-8795, Japan
[6]Department of Electronic Systems, Aalborg University, 9220 Aalborg, Denmark
[7]China Academy of Information and Communications Technology, Beijing 100191, China
[8]IMST GmbH, 47475 Kamp-Lintfort, Germany

Corresponding author: Kun Li (li.kun@awcc.uec.ac.jp)

ABSTRACT International guidelines and standards for human protection from electromagnetic fields have been revised recently. The epithelial/absorbed power density (APD) has been used as a new physical quantity for local exposure to frequencies >6 GHz, related to the temperature rise in the superficial layer. The assessment methods of APD for practical exposure scenarios are crucial for realistic exposures. This study investigates averaging methods for APD in nonplanar skin models for local electromagnetic field exposure from 10 to 90 GHz. Eight research groups compared the calculated APDs using distinct numerical approaches and postprocessing techniques. The intercomparison aimed to clarify the primary causes of variations in aspects, such as APD averaging methods, skin model structure, and types of exposure antennas. Statistical analyses reveal that the maximum differences in relative confidence intervals (RCI) due to different average methods and skin models are within 9.4% and 5.1%, respectively. In contrast, when the distance between the antenna and skin is set to 5 mm, the discrepancy attributed to the exposure antenna reaches 59.4% at 10 GHz. This difference does not exceed 9.2% under other computational conditions. Additionally, the spatially averaged APD appears to have a linear relationship with the maximum skin surface temperature elevation, based on regression analysis. The findings indicate that the variances in the spatially averaged APD are largely independent of both the APD averaging methods and skin model structures. However, they slightly depend on the antenna types used as exposure sources.

INDEX TERMS Dosimetry modeling, electromagnetic field, epithelial/absorbed power density, averaging method, nonplanar skin model, antenna array, millimeter wave exposure, standardization.

I. INTRODUCTION

The use of radio wave transmitters in millimeter wave frequencies has raised public concerns regarding the potential adverse health effects of excessive exposure to electromagnetic fields (EMFs) [1], [2], [3], [4]. Two international

The associate editor coordinating the review of this manuscript and approving it for publication was Zhengqing Yun.

© 2024 The Authors. This work is licensed under a Creative Commons Attribution-NonCommercial-NoDerivatives 4.0 License.
For more information, see https://creativecommons.org/licenses/by-nc-nd/4.0/

guidelines and standards for human protection, the IEEE International Committee on Electromagnetic Safety (ICES) and the International Commission on Nonionizing Radiation Protection (ICNIRP), revised their recommendations in 2019 and 2020 [5], [6], respectively. In one primary revision, the spatially averaged epithelial/absorbed power density (APD) served as a new internal physical quantity to set the dosimetric reference limit or basic restriction. These measures are employed to protect humans from excessive local temperature elevation owing to EMF exposure at frequencies between 6 and 300 GHz [7], [8], [9], [10], [11], [12], [13], [14], [15], [16], [17], [18], [19], [20], [21], [22], [23], [24], [25], [26], [27]. The rationale for spatially averaged APD was its good correlation with surface temperature rise; 4 cm^2 for common exposure scenarios and additional evaluation for 1 cm^2 area for beam exposures.

The IEEE ICES Technical Committee (TC) 95 formed a working group within Subcommittee 6 to address dosimetry modeling issues related to radio-frequency exposures above 6 GHz, particularly for millimeter waves. This working group aimed to examine appropriate averaging methods for APD in the superficial layer of various human skin models, which was conducted through an intercomparison study involving several global research institutes [4].

As an initial contribution of the working group, numerical errors caused by different computational methods were examined across 11 research institutes, specifically for planar skin models [4]. The findings showed that within the considered exposure scenarios, the maximum relative standard deviation of the spatially averaged APD varied between 42.6% and 16.7% over the 10-90 GHz range. This implies that when using an averaging method similar to the incident power density (IPD) in free space (as recommended by [28]), the variance in spatially averaged APD for planar skin models among different groups remains relatively minor.

In contrast, only a few research groups have investigated spatially averaged power densities for nonplanar body models [29], [30], [31], [32], [33]. Kapetanovic et al. computed the spatially averaged IPD (*s*IPD) on a spherical human head model at 3.5-100 GHz. They concluded that when out of the reactive near field above 6 GHz, the difference in the calculated *s*IPD is marginal, but increases significantly up to approximately 30% within the reactive near field [29]. Morimoto et al. clarified that the APD and IPD heating factors for a circular averaging area are conservative for near-field exposure from canonical sources at frequencies up to 300 GHz [30]. These factors are slightly affected by the relative size difference between the local exposure beam and square averaging area. Taguchi et al. investigated APD variations in seven realistic human head model types. They clarified that when averaged over 4 or 1 cm^2 area with different skin thicknesses, the maximum variations in spatially averaged APD were approximately 20% and 10%, respectively [32]. Diao et al. were the first to propose four averaging schemes for APD in nonplanar models. These were based on the direction of the absorbed power integration in locally exposed body regions above 6 GHz. Their findings suggested that for body models with curvature radii larger than 30 mm and at frequencies exceeding 20 GHz, the discrepancies in heating factors caused by different APD schemes were minimal [33]. However, these conclusions were generally drawn based on a simple two-dimensional analytical model. Although some other studies have calculated the spatially averaged APD using different parts of human body models, the relationship between the computed spatially averaged APDs and the resultant temperature elevation on the skin surface has not been extensively discussed. The point to be emphasized is that the correlation between APD and skin temperature rise is essential when discussing averaging methods. This is because spatially averaged APD was introduced to protect against excessive skin temperature increase.

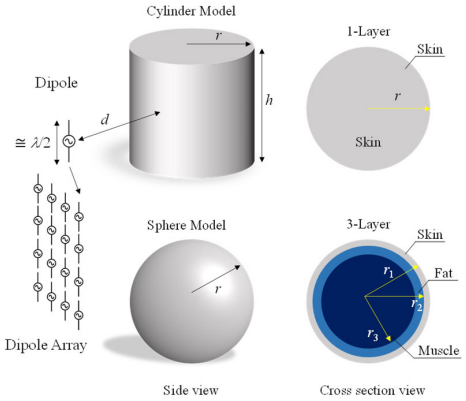

FIGURE 1. The analytical model consisting of antennas and nonplanar skin models with both one- and three-layer configurations.

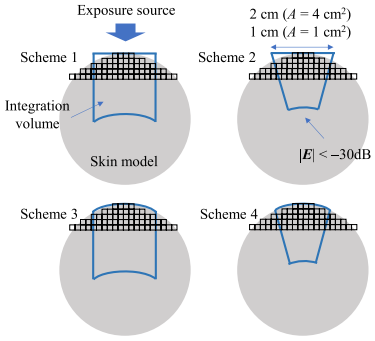

FIGURE 2. Definitions of averaging schemes available for selection.

As the second phase of the working group's efforts, this study primarily seeks to assess the variations in spatially averaged APD that arise from different average schemes for nonplanar skin models, such as cylinder and sphere models. The computational parameters for both EMF and thermal effect simulations were standardized as closely as possible. Statistical analysis was conducted to identify the principal influences of APD averaging methods, differences in analytical skin model structures, and varying antenna source types.

II. MODELS AND METHODS

This section outlines the simplified phantom of skin models, numerical methods, and computational conditions for

the intercomparison study, and provides definitions for the various APD averaging schemes.

Eight organizations collaborated in this study: Nagoya Institute of Technology (NITech), South China Agricultural University (SCAU), The University of Electro-Communications (UEC), Aalborg University (AAU), Inspiring Mobile and Satellite-communication Techniques (IMST), China Academy of Information and Communications Technology (CAICT), National Institute of Information and Communications Technology (NICT), and the University of Split (UniSt).

Both the single half-wavelength dipole and 4 × 4 dipole array antenna were employed as exposure sources following the conditions in our previous study [4], as listed in Table 1. The antenna-to-skin surface separation distance was set to the 5–10 mm range at frequencies of 10 and 30 GHz and 2–5 mm at 90 GHz. Fig. 1 shows the antennas and nonplanar skin models used for the numerical simulations. Table 2 lists the dipole lengths used by each organization. The total antenna input power was normalized to 10 mW.

Typical cylinderical and spherical models were utilized in this study to simulate the nonplanar shape of the human body. Each model has two variants: a single-layer skin model and a three-layer model consisting of the skin, fat, and muscle. Table 3 lists the cylinder model height (h) and the radius (r) for both the cylinder and sphere models. Considering the computational scale burden, we did not include the calculation of 3-layer at 90 GHz. For consistency with previous research, we adopted the same dielectric properties for each tissue layer in the skin model, as listed in Table 4 [4]. Table 4 summarizes the numerical techniques and resolutions used to evaluate the APD in nonplanar skin models.

In the numerical simulation, we first calculated the spatially averaged APD (sAPD) in the tissue using nonplanar models. In line with the ICNIRP exposure guidelines [6], each organization selected one of the two equations for deriving the sAPD, as presented in the following equations:

$$s\mathrm{APD}\,(\boldsymbol{r}) = \frac{1}{A}\iint_A \int_0^{z_{max}} \sigma\,(\boldsymbol{r})\,|\boldsymbol{E}\,(\boldsymbol{r})|^2\,dzds, \qquad (1)$$

$$s\mathrm{APD}\,(\boldsymbol{r}) = \frac{1}{A}\iint_A \mathrm{Re}\left(\boldsymbol{E}\,(\boldsymbol{r}) \times \boldsymbol{H}^*\,(\boldsymbol{r})\right)\cdot d\boldsymbol{s}, \qquad (2)$$

where $\boldsymbol{E}$ and $\boldsymbol{H}$ indicate the effective values of the complex electric and magnetic fields inside the body model, respectively; * denotes the complex conjugate; z_{max} is the depth at which the EMF is negligibly small compared to that at the skin surface; $\boldsymbol{r}$ represents the position vector; and $d\boldsymbol{s}$ is the integral variable vector. A is the average area of sAPD. All research groups were allowed to choose either equation to derive sAPD according to their own approach. Note that the difference between Eqs. (1) and (2) using planar skin models have been compared in literature [4].

We focused on four different calculation methods presented in [33] for the average schemes of sAPD in nonplanar models. As shown in Fig. 2, these methods differ based on the integration volumes represented by the blue boundaries of the polygons. The upper boundaries ran parallel to the grid axis or contour along the exposed surface. In addition, the boundaries in the depth direction of the models either run parallel to the grid axis or followed the internal electric field gradients at the model surface. The lower boundaries of the integration volume were defined by the contour at which the inner E-field strength was 30 dB below the maximum value within the integration volume. A further detailed explanation of the averaging schemes is provided in [33].

Each research organization was required to at least choose Scheme 1 for this intercomparison study and could opt for any of the remaining three average schemes. The postprocessing approach for each group was grounded in their unique techniques to ensure an objective and fair comparison.

Thermal calculations were conducted to determine the maximum temperature elevation on the skin surface up to the thermally steady state by solving the Pennes bioheat transfer equation [9], [34], [35], [36], [37], [38], [39]. The thermal parameters of each skin layer are listed in Table 5 [35]. The

TABLE 1. Exposure scenarios.

Antenna type	Skin Model	Frequency (GHz)	Distance (mm)
$\lambda/2$ dipole, 4 × 4 dipole array	Cylinder, Sphere	10	5, 10
		30	5, 10
		90	2, 5

TABLE 2. Lengths of dipole antenna elements for each organization.

Org.	10 GHz (mm)	30 GHz (mm)	90 GHz (mm)
NITech	13.75	4.25	1.25
SCAU	13.5	4.75	1.5
UEC	13.6	4.4	1.5
AAU	12.6	4.11	1.46
IMST	0.15	0.05	0.0166
CAICT	11.8	4.3	1.40
NICT	13.5	4.2	1.5/1.38
UniSt	15.0	5.0	1.67

TABLE 3. Dimensions and thicknesses of skin models at each frequency.

Skin model	Dimension	10 GHz	30 GHz	90 GHz
1-layer cylinder	r (mm)	100	50	50
	h (mm)	100	50	20
3-layer cylinder	r_1 (mm)	100	50	
	r_2 (mm)	98.5	48.5	
	r_3 (mm)	94.5	44.5	
	h (mm)	100	50	
1-layer sphere	r (mm)	100	50	50
3-layer sphere	r_1 (mm)	100	50	
	r_2 (mm)	98.5	48.5	
	r_3 (mm)	94.5	44.5	

TABLE 4. Numerical methods and spatial resolution (Δ) for numerical simulation by each organization.

Org.	Method	10 GHz (mm)	30 GHz (mm)	90 GHz (mm)
NITech	FDTD	0.25	0.25	0.05
SCAU	FDTD	0.25	0.125	0.05
UEC	FDTD	0.2	0.2	0.05
AAU	FIT	0.5	0.25	0.1
IMST	FDTD	0.15	0.05	0.0166
CAICT	FDTD	0.5	0.2	0.1
NICT	FDTD	0.5	0.25	0.1/0.125
UniSplt	GB-IBEM	0.25	0.25	0.25

TABLE 5. Thermal parameters.

Tissue	κ[W/(m·°C)]	B [W/(m^3·°C)]	ρ [kg/(m^3)]
Skin	0.42	7441	1109
Fat	0.25	1903	911
Muscle	0.5	2691	1090

details of the settings in heat transfer boundary conditions and computational conditions are consistent with our previous working group study [35].

III. RESULTS

A. COMPARISON OF SPATIALLY AVERAGED ABSORBED POWER DENSITY

Figs. 3 and 4 present the statistical analysis results of the calculated *s*APD when the average area A was set to 1 and 4 cm^2, respectively. The intercomparison data provided by all the research groups are plotted as a function of the antenna-to-skin separation distance d (in mm) at frequencies 10, 30, and 90 GHz. The red points denote the mean values, while the error bars indicate the 95% confidence intervals (CIs) of the calculated *s*APD by aggregating the results for various computation condition choices.

We analyzed the intercomparison data in terms of APD averaging methods, skin model structure, and types of exposure antennas to identify the primary cause of variance in *s*APD. The results of these analyses are shown in Figs. (a), (b) and (c), respectively. For instance, we incorporated all other influencing factors in Figs. 3 (a) and 4 (a), such as skin models and antennas. Only the effects of average schemes were compared in this configuration, as indicated by the bars. Figs. (b) and (c) follow a similar approach, with the aim of observing the differences caused by skin models and antennas. Furthermore, as mentioned in Section II, all research groups were required to calculate the *s*APD using Scheme 1. The choice among the remaining average schemes was flexible, and these selections are collectively represented as Scheme x in Figs. 3 (a) and 4 (a).

The discrepancy between Scheme 1 and x was not large across all separation distances d, frequencies, and average areas, as shown in Figs. 3 (a) and 4 (a). The absolute

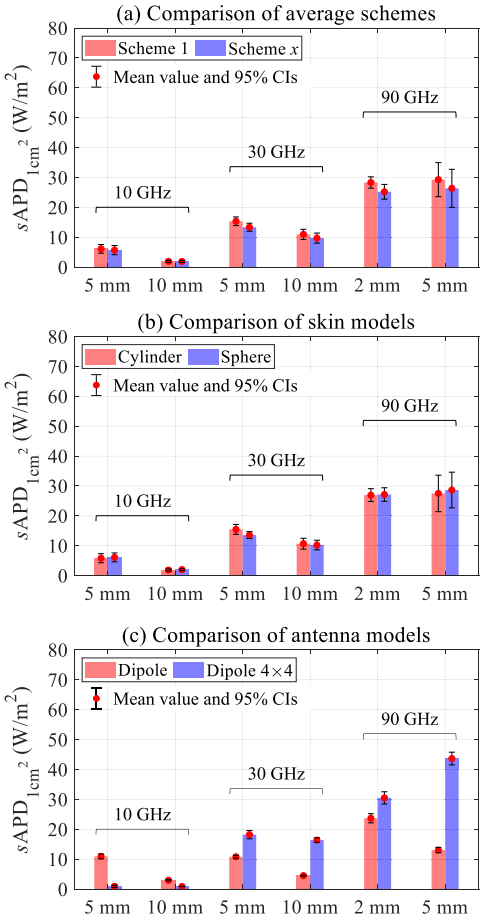

FIGURE 3. The mean value and 95% confidence intervals of spatially averaged absorbed power densities as a function of the antenna-to-skin separation distance at 10, 30, and 90 GHz when $A = 1$ cm^2. Comparisons are made based on different (a) average schemes, (b) skin models, and (c) antenna sources.

differences in the mean values between Scheme 1 and x range from 6.9% to 13.0% for $A = 1$ cm^2 and from 0.9% to 12.5% for $A = 4$ cm^2. Although the mean values for Scheme x cases might be slightly lower than those for Scheme 1 at higher frequencies, their 95% CIs largely overlap. This indicates a minimal difference in *s*APD owing to the average schemes.

Similar trends can be observed for the comparison between the skin models, i.e., cylinder and sphere models, as shown in Figs. 3 (b) and 4 (b). The absolute differences in the mean *s*APD values between Schemes 1 and x ranged from 0.6% to 12.3% for $A = 1$ cm^2, and from 1.5% to 9.6% for $A = 4$ cm^2. Notably, the difference in mean values between the cylinder and sphere models at 90 GHz is smaller than that observed with the average schemes.

Conversely, examining the impact of different exposure antenna types shows significant variations between the half-wavelength dipole and the 4 × 4 dipole array antennas across the considered separation distances d and frequencies. In Figs. 3 (c) and 4 (c), the absolute differences in the mean values between Schemes 1 and x range from 28.8% to 263.0% when $A = 1$ cm^2, and from 21.9% to 230.2% when $A = 4$ cm^2. The 95% CIs do not overlap even at the position where the

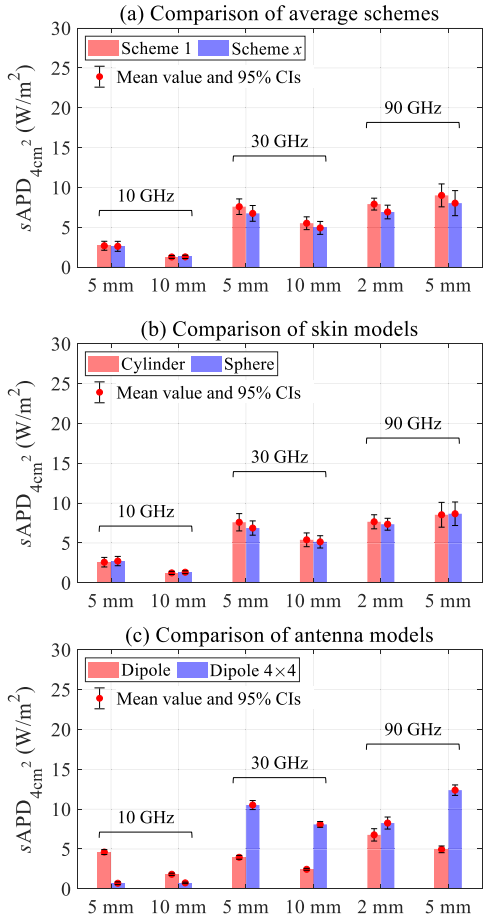

FIGURE 4. The mean value and 95% confidence intervals of spatially averaged absorbed power densities as a function of the antenna-to-skin separation distance at 10, 30, and 90 GHz when $A = 4$ cm^2. Comparisons are made based on different (a) average schemes, (b) skin models, and (c) antenna sources.

smallest deviation in mean values is observed, specifically at $d = 2$ mm at 90 GHz. This suggests that increasing the number of antenna elements might influence the calculated *s*APD much more significantly than variances in average methods or skin models.

Tables 6, 7, and 8 summarize the RCI of the calculated *s*APD for three comparison sets: average scheme, skin model, and antenna types. These correspond to the outcomes shown in Figs. 3 and 4. The percentage values in the tables were derived from the ratio of 95% CIs to their respective mean values. This measure describes the relative precision of the estimates for various datasets at the 95% confidence level.

In Table 6, the RCIs of *s*APD range between 13.4% and 47.3% for $A = 1$ cm^2 and between 18.8% and 41.9% for $A = 4$ cm^2 for average Scheme 1. For the other average schemes, the RCIs ranged between 19.5% and 53.9% for $A = 1$ cm^2 and between 24.8 % and 47.8% for $A = 4$ cm^2. It can be observed that the RCIs for Schemes 1 and x are in good agreement. The maximum difference of 9.4% occurred at $d = 5$ mm at 90 GHz when $A = 1$ cm^2.

Furthermore, as shown in Table 7, the calculated *s*APD using the cylinder skin model has RCIs ranging from 15.9% to 52.2% for $A = 1$ cm^2, and from 23.1% to 46.3% for $A = 4$ cm^2. For the sphere model, the corresponding RCIs were between 16.8% and 48.7% when $A = 1$ cm^2 and between 20.3% and 42.9% when $A = 4$ cm^2. The maximum difference of 5.1% was observed at $d = 10$ mm at 10 GHz for $A = 4$ cm^2.

Conversely, a notable increase in the difference between the RCIs can be observed when comparing the half-wavelength dipole with the dipole array antennas. As presented in Table 8, for the half-wavelength dipole, the RCIs of sAPD ranged between 6.7% and 14.3% for $A = 1$ cm^2 and between 9.7% and 22.9% for $A = 4$ cm^2. In contrast, the RCIs increased to 9.1% and 73.7% for $A = 1$ cm^2 and 9.0% and 48.9% for $A = 4$ cm^2 when using the 4×4 dipole array as the exposure source. The most pronounced difference in RCIs between these two antenna types was 59.4%, occurring at $d = 5$ mm

TABLE 6. The relative confidence interval for the comparison of *s*APD between average scheme 1 and scheme x.

		Scheme 1		Scheme x	
Freq. (GHz)	d (mm)	$sAPD_{1\,cm^2}$ (%)	$sAPD_{4\,cm^2}$ (%)	$sAPD_{1\,cm^2}$ (%)	$sAPD_{4\,cm}$ (%)^2
10	5	47.3	41.9	53.9	47.8
	10	32.2	27.4	35.6	31.8
30	5	18.8	25.8	20.1	29.3
	10	30.8	29.1	34.6	32.9
90	2	13.4	18.8	19.5	24.8
	5	38.9	31.9	48.3	39.1

TABLE 7. The relative confidence interval for the comparison of *s*APD between cylinder and sphere models.

		Cylinder Model		Sphere Model	
Freq. (GHz)	d (mm)	$sAPD_{1\,cm^2}$ (%)	$sAPD_{4\,cm^2}$ (%)	$sAPD_{1\,cm^2}$ (%)	$sAPD_{4\,cm^2}$ (%)
10	5	52.2	46.3	48.7	42.9
	10	35.9	31.9	31.8	26.8
30	5	21.5	28.6	17.0	26.1
	10	34.0	32.0	31.5	30.0
90	2	15.9	23.1	16.8	20.3
	5	44.4	36.5	41.7	34.1

TABLE 8. The relative confidence interval for the comparison of *s*APD between dipole and dipole array antennas.

		Dipole Antenna		Dipole 4×4	
Freq. (GHz)	d (mm)	$sAPD_{1\,cm^2}$ (%)	$sAPD_{4\,cm^2}$ (%)	$sAPD_{1\,cm^2}$ (%)	$sAPD_{4\,cm^2}$ (%)
10	5	14.3	13.4	73.7	48.9
	10	13.6	15.2	19.7	24.4
30	5	8.9	12.1	15.2	10.8
	10	6.7	9.7	9.1	9.0
90	2	12.9	22.9	13.4	18.3
	5	13.7	17.0	9.8	10.6

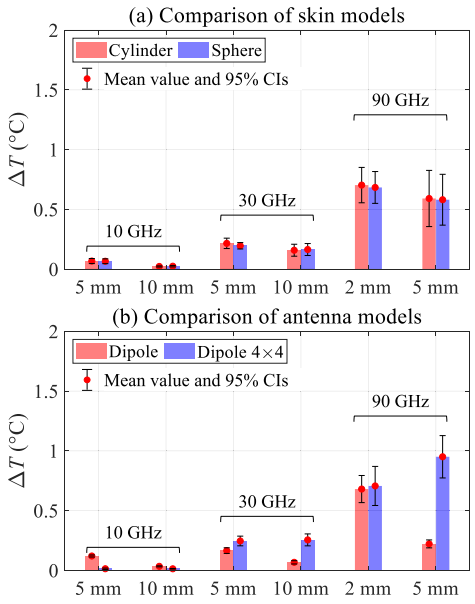

FIGURE 5. The mean value and 95% confidence intervals of maximum skin surface temperature elevation as a function of the antenna-to-skin separation distance at 10, 30, and 90 GHz. Comparisons are made based on different (a) skin models and (b) antenna sources.

at 10 GHz for $A = 1$ cm^2. Aside from this specific condition, the differences in RCI remained within 9.2%.

B. COMPARISON OF MAXIMUM TEMPERATURE ELEVATION AT SKIN SURFACE

Fig. 5 shows the statistical results of the calculated thermal-steady-state spatial-peak temperature elevation (ΔT) at the skin model surface. The mean value and 95% CI are plotted in a similar manner to those in Figs. 3 and 4. Here, only the comparison of skin models and antenna types was considered.

As shown in Fig. 5 (a), the absolute differences in the mean ΔT values between cylinder and sphere models range from 1.7% to 9.3% under the considered conditions of d and frequencies. This suggests that the variation between different shapes of simple nonplanar skin models does not significantly influence the calculated ΔT.

Conversely, distinct deviations were observed between the half-wavelength dipole and the 4 × 4 dipole array antennas when considering the differences caused by exposure antenna types. In Fig. 5 (b), the absolute differences in the mean ΔT values between these two antenna types range from 3.8% to 328.6%. The most significant discrepancies of 277.8% and 328.6% appeared at $d = 10$ mm at 30 GHz and $d = 5$ mm at 90 GHz, respectively. The maximum difference remained notably high even outside these conditions, reaching 88.5%. This result implies that the antenna type may also have a more pronounced impact on the calculated ΔT than that of the choice of skin model.

Table 9 summarizes the RCIs of the calculated ΔT for the comparison sets of skin models and antenna types, corresponding to the results in Fig. 5. As shown in Table 9, the ΔT calculated using the cylinder skin model had RCIs ranging from 40.2% to 79.5%. For the sphere model, the corresponding RCIs were between 27.3% and 73.2%. The maximum difference of 12.9% occurs at $d = 5$ mm at 30 GHz. In contrast, for cases of the dipole and dipole array antennas, the ΔT RCIs ranged from 13.8% to 40.7% and 32.9% to 80.1%, respectively. The maximum difference of 66.3% occurred at $d = 5$ mm at 10 GHz. The differences in RCIs remain within 12.9% without considering this specific condition.

TABLE 9. The relative confidence interval for the ΔT comparison.

		Cylinder Model	Sphere Model	Dipole Antenna	Dipole 4 × 4
Freq. (GHz)	d (mm)	ΔT (%)	ΔT (%)	ΔT (%)	ΔT (%)
10	5	62.1	60.7	13.8	80.1
	10	40.5	45.4	25.3	38.2
30	5	40.2	27.3	28.6	32.9
	10	63.1	60.9	40.7	39.1
90	2	42.1	39.0	33.4	46.3
	5	79.5	73.2	29.9	37.3

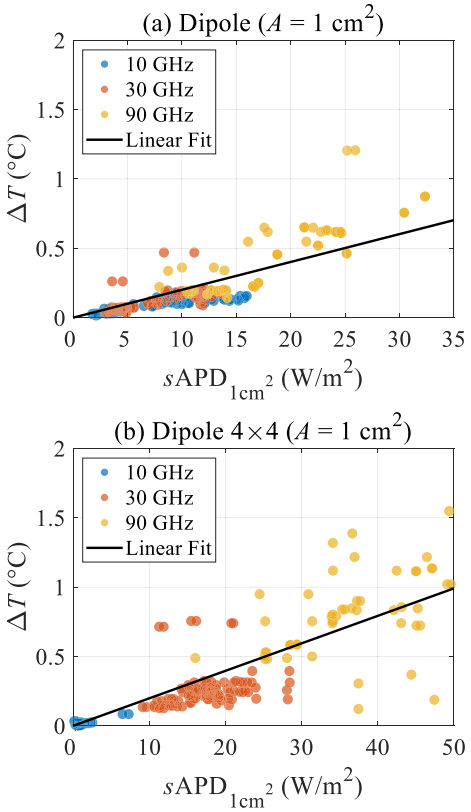

FIGURE 6. Regression analysis of skin surface temperature elevation as a function of spatially averaged epithelial/absorbed power density for a studied antenna when $A = 1$ cm^2 at 10, 30, and 90 GHz frequencies. (a) the single dipole and (b) the 4 × 4 dipole array.

C. RELATIONSHIP BETWEEN SKIN TEMPERATURE ELEVATION AND SPATIALLY AVERAGED ABSORBED POWER DENSITY

Figs. 6 and 7 represent scatter plots of all calculated ΔT values as a function of the sAPD for the average area A set to 1 cm^2 and 4 cm^2, respectively. Figs. 6 (a) and 7 (a) show the

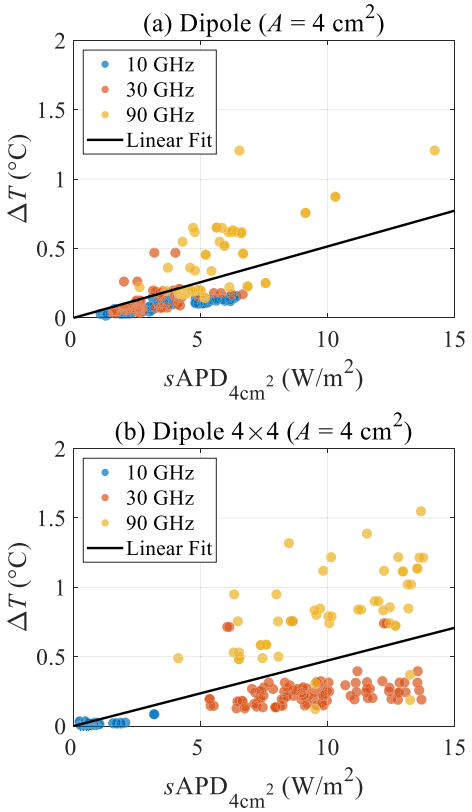

FIGURE 7. Regression analysis of skin surface temperature elevation as a function of spatially averaged epithelial/absorbed power density for a studied antenna when $A = 4$ cm^2 at 10, 30, and 90 GHz frequencies. (a) the single dipole and (b) the 4 × 4 dipole array.

TABLE 10. Regression analysis using ordinary least squares.

Conditions	Slope (°C/(W/m^2))	R^2
Dipole (A = 1 cm^2)	0.0202	0.825
Dipole 4 × 4 (A = 1 cm^2)	0.0199	0.841
Dipole (A = 4 cm^2)	0.0517	0.710
Dipole 4 × 4 (A = 4 cm^2)	0.0472	0.687

results for the single-dipole antenna, while Figs. 6 (b) and 7 (b) depict those for the 4 × 4 dipole array. The intercomparison data are plotted separately for 10, 30, and 90 GHz groups. Furthermore, the one-dimensional linear regression curve derived by least-squares methods, illustrating the relationship between ΔT and sAPD, was included.

When a single-dipole antenna is used as the exposure source, the calculated ΔT and sAPD exhibit an approximately linear relationship with each other, as shown in Figs. 6 (a) and 7 (a), which is irrespective of the average schemes, skin model structures, as well as d and frequencies. Notable deviations in the data at 90 GHz are observed because extremely close separation distances at $d = 2$ mm were included. This is corroborated by the slight deviation from the approximation lines observed at higher sAPD levels.

Conversely, as shown in Figs. 6 (b) and 7 (b), when using the 4 × 4 dipole array, the data points are more scattered compared to those when using single-dipole antennas. Deviations from the best-fitting lines are evident not only at 90 GHz, but also at 10 GHz. This might be due to the complex near-field interactions between the dipole array antennas and nonplanar skin models under the considered exposure conditions in this study.

The goodness of fit of the regression analysis based on ordinary least squares are given in Table 10 for cases of the single dipole and 4 × 4 dipole array with averaging areas A of 1 and 4 cm^2. Although subtle variations in the slope attributed to differences in antenna types and averaging areas are observed, the R^2 values for both the dipole and dipole arrays remain fairly consistent. This demonstrates a moderately strong correlation ($0.687 < R^2 < 0.841$) between ΔT and sAPD. Furthermore, an f-test was performed to assess the overall statistical significance of the regression, with the alpha level set to 0.05. In all cases, the p-value is well below this threshold level, indicating sufficient evidence to conclude that the association between ΔT and sAPD is statistically significant.

IV. DISCUSSION AND CONCLUSION

Following our previous activities on the intercomparison studies of sIPD [35] and sAPD [4], this study conducted a more in-depth analysis and comparison from three distinct perspectives:

1) Skin model curvature: We employed typical cylinder or sphere models to represent the curvature of the skin model surface, which is different from the traditional approach of using a stratified phantom, i.e., planar skin models.
2) Averaging methods: Owing to the skin surface curvature, various averaging methods have been considered according to the direction of absorbed power integration in locally exposed body regions, which needs to be summarized and compared.
3) Relationship between sAPD and steady-state temperature rise at the skin surface: This study explores the relationship between sAPD and skin surface temperature rise under diverse exposure conditions. This includes variations in averaging schemes, nonplanar skin model structures, and impacts caused by exposure antenna types.

Unlike our previous study [4], which directly compared different research groups against each other, this study places greater emphasis on statistical analysis, such as using 95% CIs and regression analysis. This ensures a thorough evaluation of the various influencing factors. The research groups were allowed more flexibility in their choice of numerical methods and average schemes for postprocessing the calculated sAPD. We believe that this approach renders our intercomparison data more objective and representative. This provides valuable insights into appropriate averaging methods for evaluating sAPD in typical nonplanar skin models. Moreover, it offers guidelines for using these average

schemes in more complex dosimetry modeling, such as voxel human models at millimeter wave bands.

The initial stage of this intercomparison segmented the analysis into three aspects to clarify the main cause of differences in the calculated *s*APD across the eight research groups: APD averaging methods, skin model structure, and types of exposure antennas. From a statistical analysis perspective, the absolute difference in the mean values when comparing the average schemes and skin models stands at 13.0% and 12.3%, respectively. In addition, considering the discrepancies in the relative 95% CIs, we observed that the peak differences in RCIs are 9.4% for averaging schemes and 5.1% for skin models. These findings demonstrate that variations in the calculated *s*APD, whether due to the averaging methods or skin models, are relatively small. However, when comparing antenna types, the absolute difference in the mean values increases to 263.0%. Concurrently, the maximum difference in RCIs rises to 48.9%. These figures indicate that selecting the antenna used as the exposure source can significantly influence the calculated *s*APD.

In the second phase of this study, we explored the variance in the ΔT caused by the difference in both the skin models and antenna types. Notably, this is the first instance of dosimetry modeling comparisons at millimeter waves for these specific nonplanar models. Our results indicated that the absolute differences in the mean ΔT values between the cylinder and sphere models were confined to 9.3%. However, when comparing the half-wavelength dipole with the 4×4 dipole array antennas, the corresponding difference increased to 328.6%. In contrast, compared to the RCIs of ΔT, the maximum difference between the cylinder and sphere models remained within 12.9%. The maximum RCI variance in ΔT increased up to 66.3% in scenarios involving the dipole and dipole array antennas. These findings suggest that, under the exposure conditions examined in this study, the antenna type may exert a greater influence on the calculated ΔT than variations in typical nonplanar skin models.

Additionally, this study offers a statistical analysis, using intercomparison data for the first time, to elucidate the relationship between calculated *s*APD and ΔT by employing nonplanar skin models and various averaging schemes. The results reveal that almost all of the intercomparison data predominantly aligns with linear fitting lines. This suggests a strong correlation between *s*APD and ΔT, regardless of utilized averaging methods or skin model structures. A slight dependency on antenna types, separation distances, and frequencies was observed under the conditions considered for dosimetry modeling at millimeter wave bands. Note that the most significant discrepancy occurs at 90 GHz when the antenna is extremely close to the human body. These conclusions strongly agree with our findings from previous working group activities [4], [35].

This study investigates the first intercomparison of calculated *s*APD and ΔT in typical nonplanar skin models concerning antenna exposure ranging from 10 to 90 GHz. It objectively evaluates the principal sources of variance in calculated *s*APD and ΔT by comparing the analysis outcomes of the eight research groups. The intercomparison results are in substantial agreement, showing minimal discrepancies in the calculated sAPD owing to average schemes using nonplanar skin models. As the number of antenna arrays increases, a mild escalation in dependency on antenna types for dosimetry modeling may be observed. This may primarily be attributed to variations in the distribution inside the averaging region.

REFERENCES

[1] A. Hirata, Y. Diao, T. Onishi, K. Sasaki, S. Ahn, D. Colombi, V. De Santis, V. De Santis, L. Giaccone, W. Joseph, E. A. Rashed, W. Kainz, and J. Chen, "Assessment of human exposure to electromagnetic fields: Review and future directions," *IEEE Trans. Electromagn. Compat.*, vol. 63, no. 5, pp. 1619–1630, Oct. 2021.

[2] T. Wu, T. S. Rappaport, and C. M. Collins, "Safe for generations to come: Considerations of safety for millimeter waves in wireless communications," *IEEE Microw. Mag.*, vol. 16, no. 2, pp. 65–84, Mar. 2015.

[3] T. Wu, R. Peng, L. Zhang, and K. Li, "Editorial: Human exposure to new-emerging electric, magnetic and electromagnetic fields," *Frontiers Public Health*, vol. 10, Apr. 2022, Art. no. 894624.

[4] K. Li, S. Kodera, D. Poljak, Y. Diao, K. Sasaki, A. Šušnjara, A. Prokop, K. Taguchi, J. Xi, S. Zhang, M. Yao, G. Sacco, M. Zhadobov, W. E. Hajj, and A. Hirata, "Calculated epithelial/absorbed power density for exposure from antennas at 10–90 GHz: Intercomparison study using a planar skin model," *IEEE Access*, vol. 11, pp. 7420–7435, 2023.

[5] *IEEE Standard for Safety Levels with Respect to Human Exposure to Electric, Magnetic, and Electromagnetic Fields, 0 Hz To 300 GHz*, IEEE Standard C95.1, New York, NY, USA, 2019.

[6] International Commission on Non-Ionizing Radiation Protection, "Guidelines for limiting exposure to electromagnetic fields (100 kHz to 300 GHz)," *Health Phys.*, vol. 118, no. 5, pp. 483–524, May 2020.

[7] K. R. Foster, M. C. Ziskin, and Q. Balzano, "Thermal modeling for the next generation of radiofrequency exposure limits: Commentary," *Health Phys.*, vol. 113, no. 1, pp. 41–53, Jul. 2017.

[8] M. C. Ziskin, S. I. Alekseev, K. R. Foster, and Q. Balzano, "Tissue models for RF exposure evaluation at frequencies above 6 GHz," *Bioelectromagnetics*, vol. 39, no. 3, pp. 173–189, Apr. 2018.

[9] A. Hirata, S. Kodera, K. Sasaki, J. Gomez-Tames, I. Laakso, A. Wood, S. Watanabe, and K. R. Foster, "Human exposure to radiofrequency energy above 6 GHz: Review of computational dosimetry studies," *Phys. Med. Biol.*, vol. 66, no. 8, Apr. 2021, Art. no. 08TR01.

[10] Y. Hashimoto, A. Hirata, R. Morimoto, S. Aonuma, I. Laakso, K. Jokela, and K. R. Foster, "On the averaging area for incident power density for human exposure limits at frequencies over 6 GHz," *Phys. Med. Biol.*, vol. 62, no. 8, pp. 3124–3138, Apr. 2017.

[11] A. Hirata, D. Funahashi, and S. Kodera, "Setting exposure guidelines and product safety standards for radio-frequency exposure at frequencies above 6 GHz: Brief review," *Ann. Telecommun.*, vol. 74, nos. 1–2, pp. 17–24, Feb. 2019.

[12] Y. Diao and A. Hirata, "Assessment of mmWave exposure from antenna based on transformation of spherical wave expansion to plane wave expansion," *IEEE Access*, vol. 9, pp. 111608–111615, 2021.

[13] D. Funahashi, A. Hirata, S. Kodera, and K. R. Foster, "Area-averaged transmitted power density at skin surface as metric to estimate surface temperature elevation," *IEEE Access*, vol. 6, pp. 77665–77674, 2018.

[14] A. Kanezaki, A. Hirata, S. Watanabe, and H. Shirai, "Parameter variation effects on temperature elevation in a steady-state, one-dimensional thermal model for millimeter wave exposure of one- and three-layer human tissue," *Phys. Med. Biol.*, vol. 55, no. 16, pp. 4647–4659, Jul. 2010.

[15] Y. Diao and A. Hirata, "Exposure assessment of array antennas at 28 GHz using hybrid spherical near-field transformation and FDTD method," *IEEE Trans. Electromagn. Compat.*, vol. 63, no. 5, pp. 1690–1698, Oct. 2021.

[16] Y. Diao, K. Li, K. Sasaki, S. Kodera, I. Laakso, W. E. Hajj, and A. Hirata, "Effect of incidence angle on the spatial-average of incident power density definition to correlate skin temperature rise for millimeter wave exposures," *IEEE Trans. Electromagn. Compat.*, vol. 63, no. 5, pp. 1709–1716, Oct. 2021.

[17] T. Nakae, D. Funahashi, J. Higashiyama, T. Onishi, and A. Hirata, "Skin temperature elevation for incident power densities from dipole arrays at 28 GHz," *IEEE Access*, vol. 8, pp. 26863–26871, 2020.

[18] K. Li, K. Sasaki, K. Wake, T. Onishi, and S. Watanabe, "Quantitative comparison of power densities related to electromagnetic near-field exposures with safety guidelines from 6 to 100 GHz," *IEEE Access*, vol. 9, pp. 115801–115812, 2021.

[19] S. Kodera, N. Miura, Y. Diao, M. Inoue, T. Hikage, K. Taguchi, H. Masuda, and A. Hirata, "Whole-body exposure system using horn antennas with dielectric lens at 28 GHz," *IEEE J. Electromagn., RF Microw. Med. Biol.*, vol. 7, no. 1, pp. 65–72, Mar. 2023.

[20] M. Yao, S. S. Zhekov, B. Xu, K. Li, and S. Zhang, "A study on exposure to electromagnetic fields from user equipment antennas above 100 GHz," *IEEE Trans. Electromagn. Compat.*, vol. 65, no. 5, pp. 1292–1299, Oct. 2023.

[21] D. Colombi, B. Thors, C. Tornevik, and Q. Balzano, "RF energy absorption by biological tissues in close proximity to millimeter-wave 5G wireless equipment," *IEEE Access*, vol. 6, pp. 4974–4981, 2018.

[22] K. Li, K. Sasaki, S. Watanabe, and H. Shirai, "Relationship between power density and surface temperature elevation for human skin exposure to electromagnetic waves with oblique incidence angle from 6 GHz to 1 THz," *Phys. Med. Biol.*, vol. 64, no. 6, Mar. 2019, Art. no. 065016.

[23] K. Li, "Multivariate regression analysis of skin temperature rises for millimeter-wave dosimetry," *IEEE Trans. Electromagn. Compat.*, vol. 64, no. 4, pp. 941–950, Aug. 2022.

[24] C. Li and T. Wu, "Efficient evaluation of incident power density by millimeter-wave MIMO user equipment using vectorized field superposition and stochastic population optimizers," *IEEE Trans. Electromagn. Compat.*, vol. 65, no. 4, pp. 1090–1097, Aug. 2023.

[25] K. Li, T. Hikage, H. Masuda, E. Ijima, A. Nagai, and K. Taguchi, "Parameter variation effects on millimeter wave dosimetry based on precise skin thickness in real rats," *Sci. Rep.*, vol. 13, no. 1, Oct. 2023, Art. no. 17397.

[26] E. Ijima, K. Li, T. Hikage, A. Nagai, Y. Murakami, T. Arima, T. Ishitake, and H. Masuda, "Intensity-dependent temperature rise induced by local exposure to 26.5 GHz quasi-millimeter-wave in rat," *Vivo*, vol. 37, no. 5, pp. 2092–2099, 2023.

[27] N. Miura, S. Kodera, Y. Diao, J. Higashiyama, Y. Suzuki, and A. Hirata, "Power absorption and skin temperature rise from simultaneous near-field exposure at 2 and 28 GHz," *IEEE Access*, vol. 9, pp. 152140–152149, 2021.

[28] *IEEE Guide for the Definition of Incident Power Density to Correlate Surface Temperature Elevation*, IEEE Standard 2889TM, Dec. 2021.

[29] A. L. Kapetanovic and D. Poljak, "Assessment of incident power density on spherical head model up to 100 GHz," *IEEE Trans. Electromagn. Compat.*, vol. 64, no. 5, pp. 1296–1303, Oct. 2022.

[30] R. Morimoto and A. Hirata, "Assessment of incident power density in different shapes of averaging area for radio-frequency exposure above 6 GHz," *Phys. Med. Biol.*, vol. 67, no. 21, Oct. 2022, Art. no. 215014.

[31] G. Sacco, Z. Haider, and M. Zhadobov, "Exposure levels induced in curved body parts at mmWaves," *IEEE J. Electromagn., RF Microw. Med. Biol.*, vol. 6, no. 3, pp. 413–419, Sep. 2022.

[32] K. Taguchi, S. Kodera, A. Hirata, and T. Kashiwa, "Computation of absorbed power densities in high-resolution head models by considering skin thickness in quasi-millimeter and millimeter wave bands," *IEEE J. Electromagn., RF Microw. Med. Biol.*, vol. 6, no. 4, pp. 516–523, Dec. 2022.

[33] Y. Diao, E. A. Rashed, and A. Hirata, "Assessment of absorbed power density and temperature rise for nonplanar body model under electromagnetic exposure above 6 GHz," *Phys. Med. Biol.*, vol. 65, no. 22, Nov. 2020, Art. no. 224001.

[34] H. H. Pennes, "Analysis of tissue and arterial blood temperatures in the resting human forearm," *J. Appl. Physiol.*, vol. 1, no. 2, pp. 93–122, Aug. 1948.

[35] K. Li, Y. Diao, K. Sasaki, A. Prokop, D. Poljak, V. Doric, J. Xi, S. Kodera, A. Hirata, and W. E. Hajj, "Intercomparison of calculated incident power density and temperature rise for exposure from different antennas at 10–90 GHz," *IEEE Access*, vol. 9, pp. 151654–151666, 2021.

[36] A. Hirata, O. Fujiwara, and T. Shiozawa, "Correlation between peak spatial-average SAR and temperature increase due to antennas attached to human trunk," *IEEE Trans. Biomed. Eng.*, vol. 53, no. 8, pp. 1658–1664, Aug. 2006.

[37] A. Hirata and O. Fujiwara, "The correlation between mass-averaged SAR and temperature elevation in the human head model exposed to RF near-fields from 1 to 6 GHz," *Phys. Med. Biol.*, vol. 54, no. 23, pp. 7227–7238, Dec. 2009.

[38] R. Morimoto, I. Laakso, V. De Santis, and A. Hirata, "Relationship between peak spatial-averaged specific absorption rate and peak temperature elevation in human head in frequency range of 1–30 GHz," *Phys. Med. Biol.*, vol. 61, no. 14, pp. 5406–5425, Jul. 2016.

[39] R. Morimoto, A. Hirata, I. Laakso, M. C. Ziskin, and K. R. Foster, "Time constants for temperature elevation in human models exposed to dipole antennas and beams in the frequency range from 1 to 30 GHz," *Phys. Med. Biol.*, vol. 62, no. 5, pp. 1676–1699, Feb. 2017.

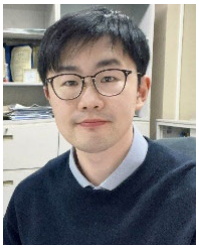

KUN LI (Member, IEEE) received the B.E. degree in communication engineering from the Nanjing University of Posts and Telecommunications, Nanjing, China, in 2011, and the M.E. and Ph.D. degrees in electrical engineering from the University of Toyama, Toyama, Japan, in 2014 and 2017, respectively.

From 2017 to 2019, he was a Researcher with the Electromagnetic Compatibility Laboratory, National Institute of Information and Communications Technology, Tokyo, Japan. From 2020 to 2023, he was an Assistant Professor with the Faculty of Engineering and Design, Kagawa University, Takamatsu, Japan. He was a Visiting Researcher with the CNRS/IETR, University of Rennes 1, Rennes, France, from 2022 to 2023. In 2023, he joined the Advanced Wireless and Communication Research Center, The University of Electro-Communications, Tokyo, where he is currently an Associate Professor. His research interests include electromagnetic computation and measurement for radiation safety by human exposure to electromagnetic fields in radio frequencies, antenna design, and measurement techniques for wireless communication systems.

Dr. Li was a recipient of the Young Scientist Award of the URSI, in 2020, the Risaburo Sato Award of EMC Sapporo & AMPEC, in 2019, the IEEE AP-S Japan Student Award, in 2015, and the IEICE Best Letter Award, in 2017. He is also an Associate Editor of IEEE ANTENNA AND WIRELESS PROPAGATION LETTERS, the Early Career Representative of URSI Commission K, and the Co-Chair of Working Group under Subcommittee 6, the IEEE International Committee on Electromagnetic Safety (ICES) TC-95. He is a Senior Member of URSI and a member of IEICE.

SACHIKO KODERA (Member, IEEE) received the B.E. and M.E. degrees in electrical and computer engineering and the Ph.D. degree in computer science from the Nagoya Institute of Technology, Nagoya, Japan, in 2002, 2006, and 2019, respectively.

In 2016, she joined the Department of Electrical and Mechanical Engineering, Nagoya Institute of Technology, where she is currently an Associate Professor. Her current research interests include electromagnetic and thermal dosimetry modeling in humans for radio frequency and ambient heat exposures.

Dr. Kodera is a member of Subcommittee 6 in Technical Committee 95 of IEEE International Committee on Electromagnetic Safety and the Scientific Expert Group of International Commission on Non-Ionizing Radiation Protection. She received the Prizes for Science and Technology (Public Understanding Promotion Category, in 2020) from the Commendation for Science and Technology, Minister of Education, Culture, Sports, Science, and Technology, Japan, and the Japan Open Innovation Prize (President of the Science Council of Japan Prize, in 2022) from the Cabinet Office.

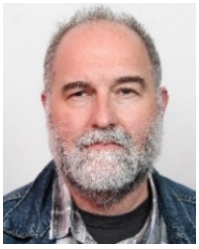

DRAGAN POLJAK (Senior Member, IEEE) received the Ph.D. degree in electrical engineering from the University of Split, Croatia, in 1996. He is currently a Full Professor with the Department of Electronics and Computing, University of Split. His research interests include computational electromagnetics (electromagnetic compatibility, bioelectromagnetics, and plasma physics). He has published more than 160 journals and 250 conference papers, and authored some books, e.g. two by Wiley, New Jersey, and one by Elsevier, St Louis. He is a member of Editorial Board of *Engineering Analysis with Boundary Elements*, *Mathematical Problems in Engineering*, and *IET Science, Measurement & Technology*. He was awarded by several prizes for his achievements, such as the National Prize for Science, in 2004, the Croatian Section of IEEE Annual Award, in 2016, the Technical Achievement Award of the IEEE EMC Society, in 2019, and the George Green Medal from the University of Mississippi, in 2021. From May 2013 to June 2021, he was a member of the board of the Croatian Science Foundation. He is also involved in ITER physics EUROfusion collaboration and in Croatian center for excellence in research for technology sciences. He is active in few Working Groups of IEEE/International Committee on Electromagnetic Safety (ICES) Technology Committee 95 SC6 EMF Dosimetry Modeling.

YINLIANG DIAO (Member, IEEE) received the B.E. degree in electronic information engineering from Chongqing University, Chongqing, China, in 2008, the M.S. degree in electronic engineering from the Beijing University of Posts and Telecommunications, Beijing, China, in 2011, and the Ph.D. degree in electronic engineering from the City University of Hong Kong, in 2016.

Since 2017, he has been an Assistant Professor with South China Agricultural University, Guangzhou, China, where he is currently an Associate Professor. In 2019, he joined the Department of Electrical and Mechanical Engineering, Nagoya Institute of Technology, where he is also a Guest Associate Professor. His current research interests include electromagnetic dosimetry modeling and electromagnetic compatibility.

Dr. Diao is a member of IEEE International Committee on Electromagnetic Safety and a member of the Scientific Expert Group of International Commission on Non-Ionizing Radiation Protection. He was a recipient of the Young Scientist Award from URSI GASS 2020.

KENSUKE SASAKI (Member, IEEE) received the B.E., M.E., and Ph.D. degrees in electrical and electronic engineering from Tokyo Metropolitan University, Tokyo, Japan, in 2006, 2008, and 2011, respectively.

He is currently a Planning Manager with the Strategic Planning Office, National Institute of Information and Communications Technology, Japan. He has been a Visiting Associate Professor with the Nagoya Institute of Technology, Japan, since 2022. His research interests include electromagnetic theory, bioelectromagnetics, and dielectric properties measurement.

Dr. Sasaki was a member of the Scientific Expert Group of International Commission on Non-Ionizing Radiation Protection (ICNIRP), from 2018 to 2020. He was a recipient of the 2009 Young Scientist Award of the URSI, the 2012 Best Paper Award of the IEEJ, and the 2020 Achievement Award of the IEICE. He was the Early Carrier Representative of Commission K, the International Scientific Radio Union (URSI), from 2017 to 2023. He has been the Co-Chair of Working Group 6 under Subcommittee 6, the IEEE International Committee on Electromagnetic Safety (ICES) TC-95, since 2022.

SHUAI ZHANG (Senior Member, IEEE) received the B.E. degree from the University of Electronic Science and Technology of China, Chengdu, China, in 2007, and the Ph.D. degree in electromagnetic engineering from the Royal Institute of Technology (KTH), Stockholm, Sweden, in 2013. After the Ph.D. degree, he was a Postdoctoral Researcher with KTH. In April 2014, he joined Aalborg University, Denmark, where he is currently an Associate Professor and the Head of Antenna Research Group. In 2010 and 2011, he was a Visiting Researcher with Lund University, Sweden, and Sony Mobile Communications AB, Sweden, respectively. He was also an External Antenna Specialist with Bang & Olufsen, Denmark, from 2016 to 2017. He has coauthored over 100 articles in well-reputed international journals and over 16 (US or WO) patents. His current research interests include mmwave antennas for cellular communications, biological effects, metasurfaces, CubeSat antennas, massive MIMO antenna arrays, wireless sensors, and RFID antennas.

MING YAO (Graduate Student Member, IEEE) was born in 1994. He received the B.Eng. and M.Eng. degrees from the University of Electronic Science and Technology of China, Chengdu, China, in 2017 and 2020, respectively. He is currently pursuing the Ph.D. degree in wireless communication with the Antennas, Propagation, and Millimeter-Wave Systems Section, Department of Electronic Systems, Aalborg University, Aalborg, Denmark. His current research interests include antenna design, holographic metasurface, EMF health, and safety.

ANTE KAPETANOVIC (Member, IEEE) was born in Split, Croatia, in 1995. He received the B.S., M.S., and Ph.D. degrees in electrical engineering from the Faculty of Electrical Engineering, Mechanical Engineering, and Naval Architecture, University of Split, Split, in 2017, 2019, and 2023, respectively. He is currently a Junior Researcher with the University of Split. His research interests include human exposure to radio-frequency electromagnetic fields, electromagnetic and thermal dosimetry and computational bioelectromagnetics in general. He was a Research Intern with Aalborg University, Aalborg, Denmark, during the M.S. degree, in 2019, and two times a short-term Visiting Researcher with IETR/CNRS, Rennes, France, in 2021 and 2022. He was a recipient of the Best Student Paper Award at the IEEE MTT-S International Microwave Biomedical Conference in Sozhou, China, in 2022. He has been a member of the Croatian Chapter of the IEEE Electromagnetic Compatibility Society, since 2020, and a member of the BioEM, since 2021. He is also an active member of the IEEE Working Group on Power-Density Averaging within the International Committee on Electromagnetic Safety (ICES), Technical Committee 95, Sub-Committee 6 on electromagnetic field dosimetry modeling. He is also a working member of the TE-007 Technical Committee for the Australian and New Zealand standard on principles and measurement methods for human exposure to radio-frequency fields (AS/NZS 2772.2).

CONGSHENG LI (Member, IEEE) received the B.S. degree in electronic information engineering from Beijing City University, Beijing, China, in 2009, the M.S. degree in signal and information system from Beijing Information Science and Technology University, Beijing, in 2012, and the Ph.D. degree in communication and information systems from the University of Science and Technology Beijing, China, in 2015.

Since 2015, he has been an Engineer and a Senior Engineer with the China Academy of Information and Communications Technology, Beijing. His research interests include computational electromagnetics and artificial intelligence.

TONGNING WU (Senior Member, IEEE) received the B.S. degree in biomedical engineering from Tianjin University, Tianjin, China, in 2002, the M.S. degree in communication and information system from the China Academy of Telecommunication Technology, Beijing, China, in 2005, and the Ph.D. degree in électronique, traitement du signal from Université Paris-Est, Marne-la-Vallée, France, in 2009.

Since 2009, he has been an Engineer, a Senior Engineer, and a Professorate Senior Engineer with the China Academy of Information and Communications Technology. His research interests include the development of anatomical human model for electromagnetic dosimetry, and the neurological effect by human exposure to electric and electromagnetic fields.

THORSTEN LIEBIG received the Diploma degree in electrical engineering from the University of Duisburg-Essen, in 2007.

Since 2007, he has been a Research Assistant with the Department of General and Theoretical Electrical Engineering, University of Duisburg-Essen, on innovate antenna designs for 7T-MRI applications and FDTD simulation and SAR evaluation. Since 2014, he has been with the Antennas and EM Modeling Team, IMST GmbH, Kamp-Lintfort. He is a part of the core EMPIRE-XPU development team and contributes to several IEEE/IEC TC106 working groups.

WINFRIED SIMON received the degree in electrical engineering from the University of Duisburg, in 1997. He started working as a Research Assistant with the Microwave Department, IMST GmbH, Kamp-Lintfort. In 2003, he moved to the Antennas and EM Modeling Department as a Senior Engineer. He is currently the Technical Director of the EM Modeling Team and responsible for the EMPIRE-XPU development. His research interests include electromagnetic simulations, the design of millimeter wave antennas and RF front ends, and EMF health and safety. He is a Board Member of the European School of Antennas (ESoA) and contributes, since 2006, to several IEEE/IEC TC106 working groups.

AKIMASA HIRATA (Fellow, IEEE) received the B.E., M.E., and Ph.D. degrees in communications engineering from Osaka University, Suita, Japan, in 1996, 1998, and 2000, respectively.

From 1999 to 2001, he was a Research Fellow of the Japan Society for the Promotion of Science, and a Visiting Research Scientist with the University of Victoria, Victoria, BC, Canada, in 2000. In 2001, he joined the Department of Communications Engineering, Osaka University, as an Assistant Professor. In 2004, he joined as an Associate Professor with the Department of Computer Science and Engineering, Nagoya Institute of Technology, where he is currently a Full Professor. His research interests include electromagnetic safety, risk management system for heat-related illness, methods in neuroscience, antennas, and related computational techniques.

Prof. Hirata is an Editorial Board Member of physics in medicine and biology, a member of the Main Commission and the Chair of Project Group of International Commission on Non-Ionizing Radiation Protection, and a member of Administrative Committee and a Subcommittee (EMF Dosimetry Modeling) Chair of IEEE International Committee on Electromagnetic Safety, and an Expert of World Health Organization. From 2006 to 2012, he was also an Associate Editor of the IEEE TRANSACTIONS ON BIOMEDICAL ENGINEERING. He received several awards, including the Young scientists' Prize, in 2006, and Prizes for Science and Technology (Research Category, in 2011, and Public Understanding Promotion Category, in 2014 and 2020) by the Commendation for Science and Technology by the Minister of Education, Culture, Sports, Science, and Technology, Japan, and IEEE EMC-S Technical Achievement Award, in 2015, and the Richard R. Stoddart Award for Outstanding Performance, in 2023, the Japan Academy Medal and JSPS Prize, in 2018, and the Japan Open Innovation Prize (President of the Science Council of Japan Prize, in 2022) from the Cabinet Office. He is a fellow of the Institute of Physics, AAIA, and IEICE, and a member of IEE Japan, and Bioelectromagnetics Society.